Hindawi
Shock and Vibration
Volume 2019, Article ID 8314898, 12 pages
https://doi.org/10.1155/2019/8314898

Research Article

Vibration Control of Blade Section Based on Sliding Mode PI Tracking Method and OPC Technology

Tingrui Liu

College of Mechanical & Electronic Engineering, Shandong University of Science & Technology, Qingdao 266590, China

Correspondence should be addressed to Tingrui Liu; liutingrui@sdust.edu.cn

Received 10 April 2019; Accepted 11 June 2019; Published 27 June 2019

Academic Editor: Luca Pugi

Vibration control of the blade section of a wind turbine is investigated based on the sliding mode proportional-integral (SM-PI) method, i.e., sliding mode control (SMC) based on a PI controller. The structure is modeled as a 2D pretwisted blade section integrated with calculation of structural damping, which is subjected to flap/lead-lag vibrations of instability. To facilitate the hardware implementation of the control algorithm, the SM-PI method is applied to realize tracking for limited displacements and velocities. The SM-PI algorithm is a novel SMC algorithm based on the nominal model. It combines the effectiveness of the sliding mode algorithm for disturbance control and the stability of PID control for practical engineering application. The SM-PI design and stability analysis are discussed, with superiority and robustness and convergency control demonstrated. An experimental platform based on human-computer interaction using OPC technology is implemented, with position tracking for displacement and control input signal illustrated. The platform verifies the feasibility and effectiveness of the SM-PI algorithm in solving practical engineering problems, with online tuning of PI parameters realized by applying OPC technology.

1. Introduction

Vibration control for flutter instability of a wind turbine blade using intelligent control theory or structural control method is playing an important role in the field of flutter suppression for a long time. The 2D typical cross-sectional analysis has widely been used in a quick study of flap/lead-lag or flap/twist vibrations of a wind turbine blade due to its simplicity and convenience [1–3]. The analysis of various intelligent proportional-integral-derivative (PID) control theories for divergent instability control of the wind turbine blade section subjected to combined flap/lead-lag motions was investigated [1]. Some structural control methods, based on trailing-edge flaps or microtabs, were used for aeroelastic control of the cross sections [2, 3]. A numerical study on the closed-loop control of transonic buffet suppression by using a trailing-edge flap was performed [2], which was designed to solve the flutter problem. Numerical investigation of the flap/twist vibration model of a smart turbine section with a microtab was also performed in [3]. Stall flutter control of the blade section undergoing asymmetric limit oscillations was investigated by using the microtab control scheme [3]. Some other intelligent algorithms have recently been used in stability control of the wind turbine blade or flexible beam structure [4–7]. Two types of model prediction control (MPC) algorithms [4–6] were investigated to suppress the sectional vibrations of the turbine blade. The structure was modeled as 2D pretwisted cross section which incorporated the structural damping under different pretwisted angles, with vibration control investigated by using the intelligent MPC algorithm [4]. The SMC algorithm with PID sliding surface was also used to design a controller for a two-link flexible beam structure to track the chaotic signal in the presence of bounded disturbances and to regulate the tip deflection [7]. In addition, the stability of integral SMC was analyzed using the Lyapunov stability criterion to make reduction in cost of wind energy from wind turbines [8].

Rotor blades, as one of the most critical components in a wind turbine system, should maintain structural integrity. However, structural failure accidents of wind turbine blades are not uncommon. Structural failures of large wind turbine blades observed in recent years have mostly been attributed to severe divergent vibrations in flap/lead-lag directions. It is reported that with an estimated 700 thousand blades in operation globally, there are, on average, 3,800 incidents of blade failure each year [9]. Driven by the quasi-steady aerodynamic forces proposed in [10], the damping blade was described in order to study the divergent instability control by using intelligent control theory in the present study. Because SMC is one of the effective nonlinear robust approaches with respect to system dynamics and invariant to uncertainties [8], the Lyapunov stability approach is always used in SMC to keep the nonlinear system under control, and SMC method integrated with the Lyapunov analysis is used to realize the vibration control in blade sectional movements in the present study.

In view of the fact that the large wind power system is mostly controlled by PLC, the intelligent control algorithms should be analyzed in advance to facilitate execution in PLC hardware. Therefore, exploring the real-time realization of SMC has practical significance in engineering. Chakrabarty and Bartoszewicz [11] presented a theoretical analysis to show that increased robustness can be achieved for discrete SMC systems by choosing the sliding variables or the outputs. To avoid the chattering problem in the reaching-law-based discrete SMC and the generation of over-large control action in the equivalent-control-based discrete SMC, a new discrete SMC method based on nonsmooth control was proposed in [12]. As for the control of external disturbances and uncertain systems, a discrete SMC was presented for the robust chaos suppression of the generalized continuous-time chaotic systems subject to matched/mismatched disturbances in [13, 14], with a robust output feedback controller proposed for a class of uncertain discrete time, multi-input/multioutput, and linear systems. The controller was based on the combination of discrete SMC and Kalman estimator, ensuring the stability and robustness with an output tracking against the modeling uncertainties at large sampling periods.

All of these discrete SMC algorithms are used for the real-time implementation of intelligent control theory in controller hardware. However, due to the complexity of the algorithm itself, some discrete algorithms are still not suitable for implementation in general PLC hardware. In the present study, an SMC algorithm based on the nominal model, more suitable for error tracking and disturbance loads, is investigated to control divergent vibrations of the blade section. Since the PID algorithm is easy to be combined with SMC as mentioned above [7] and easy to be executed in the PLC controller, the expansion algorithm of nominal SMC based on PI controller is further applied to make use of the experiment to verify the effectiveness of the control algorithm in the present study. An experimental platform based on human-computer interaction is implemented to verify the algorithm effectiveness, with the PI controller executed in PLC hardware using OPC technology that was originally demonstrated in [15].

2. Structural Model

Figure 1 shows the coordinate system of pretwisted blade sections of the wind turbine. Figure 1(a) shows the section without pretwist, which is suspended by using the linear springs and viscous dampers located at the elastic axis EA. Figure 1(b) shows the pretwisted section of Figure 1(a). The movements of the independent airfoil section exhibit two directions of displacements. The first is the flap-wise vibration displacement perpendicular to the plane of rotation, denoted by z; and the second is the displacement of the lead-lag vibration in the rotor plane, denoted by y. The origin of the rotating axis system is located at the rigid root. The characteristic cross-sectional dimension chord length is $c = 1.316$ m at a distance $r = 5$ m from the hub. The wind velocity is denoted by $U = 10\ \mathrm{m{\cdot}s^{-1}}$. The length of the blade is $L = 15$ m, with the rotating speed being $\Omega = \lambda U/L = 2U/L$. Consider the pretwisted angle of $\theta = (r/L) \times (\pi/3)$, and the sectional equations of motions are expressed as [10, 16]

$$\begin{bmatrix} 1 & 0 \\ 0 & 1 \end{bmatrix} \begin{bmatrix} \ddot{y} \\ \ddot{z} \end{bmatrix} + \Omega C_s \begin{bmatrix} \dot{y} \\ \dot{z} \end{bmatrix} + \Omega^2 K_{sw} \begin{bmatrix} y \\ z \end{bmatrix} = \frac{c\rho_a (\Omega^2 r^2 + U^2)}{2\rho_b r} \begin{bmatrix} C_D \cos(\Psi) - C_L \sin(\Psi) + d_y \\ C_D \sin(\Psi) + C_L \cos(\Psi) + d_z \end{bmatrix}, \tag{1}$$

where the mass per length of the blade section is described by $\rho_b = 7.598\ \mathrm{kg{\cdot}m^{-1}}$; the air density is ρ_a; the natural angular frequencies of motions perpendicular to chordwise direction and parallel to chordwise direction are described by $\omega_n = 4\ \mathrm{rad{\cdot}s^{-1}}$ and $\omega_t = 8\ \mathrm{rad{\cdot}s^{-1}}$, respectively; and the corresponding damping ratios are denoted by $\xi_n = 0.02$ and $\xi_t = 0.04$, respectively. The incoming angle is $\psi = \mathrm{atan}(U/\Omega/r)$. The aerodynamic lift coefficient and drag coefficient are described as C_L and C_D, respectively. In particular, the "z" and "y" in equation (1) are defined as the flapping angle and lagging angle [16], which are called as "flap-wise" and "lead-lag wise" displacements in the present study, respectively. In addition, each order derivative term is defined as a derivative relative to a kind of reduced time.

The structural damping coefficient matrix C_s and structural stiffness coefficient matrix K_{sw} can be written as [10, 16]

$$C_s = T_{-\theta} C_{s0} T_\theta^T, \qquad K_{sw} = K_s + \begin{bmatrix} 1 & 0 \\ 0 & 1 \end{bmatrix}, \tag{2}$$

where the structural damping-based coefficient matrices can be defined as

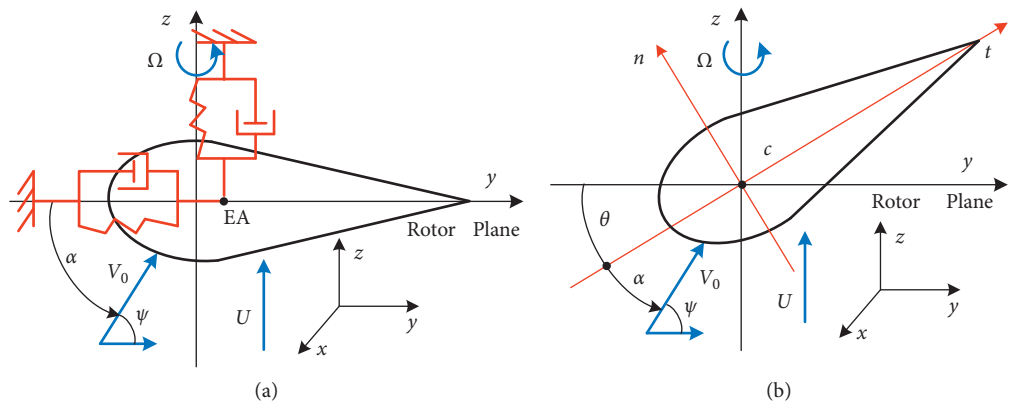

Figure 1: Coordinate system of blade sections. (a) Without pretwist. (b) Pretwisted section.

$$T_{-\theta} = \begin{bmatrix} \cos(\theta) & -\sin(\theta) \\ \sin(\theta) & \cos(\theta) \end{bmatrix},$$

$$C_{s0} = \begin{bmatrix} \frac{2\xi_t \omega_t}{\Omega} & 0 \\ 0 & \frac{2\xi_n \omega_n}{\Omega} \end{bmatrix}, \tag{3}$$

$$K_s = T_{-\theta} K_{s0} T_\theta^T = T_{-\theta} \begin{bmatrix} \frac{\omega_t^2}{\Omega^2} & 0 \\ 0 & \frac{\omega_n^2}{\Omega^2} \end{bmatrix} T_\theta^T.$$

The accuracy of the aerodynamic data is important to the analysis of the dynamic behavior of the blade section. The aerodynamic data can be obtained by using Xfoil software [10]. The lift coefficient C_L and the drag efficient C_D, each can be fitted (according to the acquired data) as a function of attack angle α in present study. The function is expressed as the Fourier series based on the first eight harmonics signals, $a_0 + \sum_{i=1}^{8} [a_i \cos(i\alpha w) + b_i \sin(i\alpha w)]$, the coefficient parameters which can be found in Table 1. The values in Table 1 satisfy the goodness of fit, with the maximum SSE being 0.1448, the minimum R-square being 0.9909, and the maximum RMSE being 0.07611. The numerical fitting method can simplify the calculation of nonlinear aerodynamic forces on the right side of equation (1), and hence equation (1) can be linearized so as to facilitate the subsequent realization of sliding mode control. The perturbed disturbance loads d_y and d_z defined later using the equivalent method are attached to the aerodynamic forces in order to study the divergent instability control more effectively in the present study.

In order to carry on the subsequent analysis, equation (1) needs to be transformed into the controlled object equation:

$$M_0 \ddot{x} + C_0 \dot{x} + G_0(x) = \tau, \tag{4}$$

where $x = [z \cdot y]^T$ is the state variable vector. τ is an extracontrol force. M_0 and C_0 are the corresponding coefficient matrices, which depend on mass coefficient and damping coefficient in equation (1). $G_0(x)$ is a variable, including stiffness term and aerodynamic term in equation (1).

Table 1: The coefficient parameters in the Fourier series model.

Coefficients	C_L	C_D
a_0	0.04848	0.6831
a_1	0.09088	−0.7148
b_1	0.08605	0.000676
a_2	0.02814	0.05465
b_2	0.8177	0.00325
a_3	−0.009271	0.006466
b_3	0.09812	0.0202
a_4	−0.01879	0.01664
b_4	0.2517	0.006258
a_5	−0.004838	0.004552
b_5	0.07703	0.02497
a_6	−0.007124	−0.01669
b_6	0.1567	−0.000389
a_7	−0.006955	−0.007571
b_7	0.07768	0.01586
a_8	−0.01469	−0.0387
b_8	0.09463	0.002131
w	1.0070	2.0090

Due to unstable aerodynamic forces in actual engineering, the coefficients matrices are usually inaccurate and can be expressed as

$$\begin{aligned} M &= M_0 + E_M, \\ C &= C_0 + E_C, \\ G(x) &= G_0(x) + E_G, \end{aligned} \tag{5}$$

where E_M, E_C, and E_G are the equivalent nominal perturbed disturbance, respectively, which is originated from the perturbed disturbance loads d_y and d_z and can be defined as $E_M = 0.2M_0 \times \text{rand}(4)$, $E_C = 0.2C_0 \times \text{rand}(4)$, and $E_G = 0.2G_0(x) \times \text{rand}(4)$. Herein, $\text{rand}(4)$ refers to the uniform distribution in the [0, 1] interval.

3. Design of Nominal SM-PI Controller

The SM-PID algorithm is a novel SMC algorithm based on the nominal model. It combines the effectiveness of the

sliding mode algorithm to disturbance control and the stability of PID control.

Let the variable tracking error be defined as $e(t) = x_d(t) - x(t)$. Herein, $x_d(t)$ is the theoretical position signal, and $x(t)$ is the actual position signal. Then, the sliding mode function can be defined as

$$r = \dot{e} + \Lambda e, \tag{6}$$

where $\Lambda > 0$.

Let $\dot{x}_r = r(t) + \dot{x}(t)$, then

$$\ddot{x}_r = \dot{r}(t) + \ddot{x}(t),\ \dot{x}_r = \dot{x}_d + \Lambda e, \ddot{x}_r = \ddot{x}_d + \Lambda \dot{e}, \tag{7}$$

and from equations (4) and (5), there exists

$$\begin{aligned} \tau &= M\ddot{x} + C\dot{x} + G(x) \\ &= M(\ddot{x}_r - \dot{r}) + C(\dot{x}_r - r) + G \\ &= M\ddot{x}_r + C\dot{x}_r + G - M\dot{r} - Cr \\ &= M_0\ddot{x}_r + C_0\dot{x}_r + G_0 + E - M\dot{r} - Cr, \end{aligned} \tag{8}$$

where $E = E_M\ddot{x}_r + E_C\dot{x}_r + E_G$. Herein, M_0, C_0, and G_0 are the nominal values of M, C, and G, respectively.

The nominal SM-PID controller can be designed as

$$\tau = \tau_m + K_p r + K_i \int r dt + K_d\left(\frac{dr}{dt}\right) + \tau_\tau, \tag{9}$$

where $K_p > 0$ and $K_i > 0$ are the proportional and integral parameters, respectively, in the PID controller. Note that, in the simulation process, the fluctuation of the two controlled displacements does not need to be sharp. This is because the derivative of the object x_d being traced (Table 2) is within a small range of [−0.1, 0.1]. Hence in the PID controller, differential control can be omitted in order to reduce the complexity of processing, i.e., let $K_d = 0$. Therefore, the nominal SM-PID controller is then degenerated into a SM-PI controller. τ_m is the control law based on the nominal model and τ_τ is the robust term, which can be described as

$$\begin{aligned} \tau_m &= M_0\ddot{x}_r + C_0\dot{x}_r + G_0, \\ \tau_\tau &= K_r \operatorname{sgn}(r), \end{aligned} \tag{10}$$

where $K_r = \operatorname{diag}[k_{rii}]$, $k_{rii} \geq |E_i|$, $i = 1, \ldots, n$.

From the above analysis of equations (8)–(10), the following can be obtained:

$$\begin{aligned} &M_0\ddot{x}_r + C_0\dot{x}_r + G_0 + E - M\dot{r} - Cr + E + \tau_\tau \\ &\quad = M_0\ddot{x}_r + C_0\dot{x}_r + G_0 + K_p r + K_i \int r dt + K_r \operatorname{sgn}(r), \end{aligned} \tag{11}$$

hence, there exists

$$M\dot{r} + Cr + G_0 + K_i \int r dt = -K_p r - K_r \operatorname{sgn}(r) + E. \tag{12}$$

4. Stability Analysis of SM-PI Controller

As mentioned in Introduction, Lyapunov theory is often used to realize stability analysis in SMC control. The Lyapunov function based on the integral type is designed as [17]

Table 2: Simulation parameters and controller parameters.

Items	Parameters
Initial conditions	(0.09–0.09)
Sampling time	0.01s
Simulation solver	ODE23tb
K_{p0}	100
K_{i0}	0.02
K_{r0}	15
Λ_0	5
Ideal position signal $x_d(1)$ for y	$0.05\sin(\pi/2t)$
Ideal position signal $x_d(2)$ for z	$0.1\sin(\pi/2t)$

$$V = \frac{1}{2}r^T M r + \frac{1}{2}\left(\int_0^t r\, d\tau\right)^T K_i \int r d\tau, \tag{13}$$

then,

$$\dot{V} = \frac{1}{2}r^T\left[M\dot{r} + \frac{1}{2}\dot{M}r + K_i \int r d\tau\right]. \tag{14}$$

Considering the orthogonality of flap-wise motion and lead-lag motion, approximately, there exists $r^T(\dot{M} - 2C)r = 0$; then,

$$\dot{V} = \frac{1}{2}r^T\left[M\dot{r} + Cr + K_i \int r\, d\tau\right]. \tag{15}$$

Inserting equation (10) into equation (15), the following equation holds:

$$\begin{aligned} \dot{V} &= -r^T K_p r - r^T K_r \operatorname{sgn}(r) + r^T E = -r^T K_p r \\ &\quad - \sum_{i=1}^{n} k_{rii}|r|_i + r^T E, \end{aligned} \tag{16}$$

since $k_{rii} \geq |E_i|$, then the following inequality holds:

$$\dot{V} \leq -r^T K_p r \leq 0, \tag{17}$$

and the convergence analysis is as follows [17]:

From equation (17), the following can be seen:

$$\lambda_{\min}\left(K_p\right)\int_0^t r^T r\, d\tau \leq \int_0^t r^T K_p r\, d\tau \leq V(0), \tag{18}$$

where $\lambda_{\min}(K_p)$ is the minimum eigenvalue of K_p.

Since $V(0) > 0$, $\lambda_{\min}(K_p) > 0$, and both items are real numbers, then $r \in L_2^n$; hence, $e \in L_2^n \cap L_\infty^n$, and when e is continuous and $t \longrightarrow \infty$, there exists $e \longrightarrow 0$, $\dot{e} \in L_2^n$.

According to equation (17), there exists $0 \leq V \leq V(0)$, $\forall t \geq 0$, and then $V(t) \in L_\infty 0$; hence, it proves that $\int_0^t r\, d\tau$ is bounded. Since $e \in L_2^n \cap L_\infty^n$, $\dot{e} \in L_2^n$, and $\dot{x}_d, \ddot{x}_d \in L_\infty^n$, there exists $\dot{x}_r$, $\ddot{x}_r \in L_\infty^n$. Consider $r \in L_2^n$; x_d, and $\tau_r \in L_\infty^n$, and then from equations (9) and (11), there exists $\dot{r}$, $\tau \in L_\infty^n$.

Since $r \in L_2^n$ and $\dot{r} \in L_\infty^n$, when $t \longrightarrow \infty$, $r \longrightarrow 0$ exists, and then it can be affirmed that when $t \longrightarrow \infty$, there $\dot{e} \longrightarrow 0$ exists. Hence, the convergence can be affirmed.

5. Numerical Simulation and Discussion

The related parameter values of the divergent instability system, including structural parameters and external motion

parameters, follow the values given in the Section 2. To realize simulation in MATLAB, the simulation parameters and the controller parameters are displayed in Table 2. Let $K_p = K_{p0}\mathrm{eye}(2)$, $K_i = K_{i0}\mathrm{eye}(2)$, $K_r = K_{r0}\mathrm{eye}(2)$, and $\Lambda = \Lambda_0\mathrm{eye}(2)$, the first two most important parameters should be determined first. Since the controlled object in the present study is divergent and has unstable displacement, it is necessary to increase the adjustment of the maximum overshoot, so K_{p0} needs a larger value, and this study focuses on tracking performance rather than attenuation; therefore, a weaker integral control is needed. Therefore, the initial values of K_{p0} and K_{i0} can be approximately determined artificially, and the precise tuning of PI parameters ($K_{p0} = 100$ and $K_{i0} = 0.02$) can be obtained by debugging the control panel of PID regulation built-in PLC using OPC technology (Section 6). Other parameters are not very sensitive to the results and can be properly valued based on experience. Because the superiority of this SM-PI algorithm lies in error tracking, two ideal displacements, flap(z) and lead-lag(y), are preset as ideal sinusoidal signals (Table 2) in advance.

Figure 2 shows the uncontrolled divergent displacements and velocities of flap(z)/lead-lag(y) motions. Displacements and velocities are both divergent and unstable. As time goes on, the blade might undergo fracture failure in the direction of flap-wise motion or lead-lag motion. In particular, the lead-lag(y) motion shows a greater divergence, which will cause greater damage in the actual operation of the blade. Achieving the boundedness of displacement fluctuation and vibration amplitude is exactly the purpose of SM-PI control.

Figure 3 demonstrates the controlled displacements and velocities of flap(z)/lead-lag(y) motions against ideal position signals, and the signals of control inputs for both flap(z)/lead-lag(y) motions. Compared with the uncontrolled displacements and velocities in Figure 2, the controlled displacements (position signal tracking curves) and velocities (speed signal tracking curves) under control in Figure 3 demonstrate obvious uniform smaller vibration amplitudes, and the positions are just within the ranges of the preset values (0.1 m and 0.05 m) in Table 2. In particular, good tracking effects have been achieved for both lead-lag(y) and flap(z) motions, which reflects the accuracy of the SM-PI tracking algorithm.

Another more significant feature from multiple repetitions of simulation is that, with respect to different preset amplitudes of both flap(z) and lead-lag(y) within range of [0.05, 0.1], the SM-PI algorithm exhibits a uniform good flutter suppression performance, which further validates the effectiveness of the SM-PI algorithm.

As for signals of control inputs in Figure 3, the fluctuation law and amplitudes are within the operational range, which also reflects the stability of the controller itself.

5.1. Superiority of SM-PI Algorithm. Another nominal SMC algorithm based on the upper bound method [17] was developed to control instability. Compared with the conventional sliding mode control, it is a better SMC algorithm based on the nominal model. The design process of the control law and effectiveness are as follows.

The Lyapunov function was designed as

$$V = \frac{1}{2} r^T M r, \tag{19}$$

then

$$\begin{aligned}\dot{V} &= \frac{1}{2} r^T \left[(\dot{M} - 2C) r + r^T C r + r^T M \dot{r}\right] \\ &= r^T (C r + M \dot{r}) = r^T \left[C r + M (\ddot{e} + \Lambda \dot{e})\right] \\ &= r^T \left[C r + M (\ddot{x}_d - \ddot{x}) + M \Lambda \dot{e}\right] \\ &= r^T \left[C \dot{e} + C \Lambda e + M \ddot{x}_d + C \dot{x} + G - \tau + M \Lambda \dot{e}\right] \\ &= r^T \left[C (\dot{x}_d + \Lambda e) + M (\ddot{x}_d + \Lambda \dot{e}) + G - \tau\right].\end{aligned} \tag{20}$$

The control law was described as

$$\tau = M_0 (\ddot{x}_d + \Lambda \dot{e}) + C_0 (\dot{x}_d + \Lambda e) + G_0 + K_r \,\mathrm{sgn}(r), \tag{21}$$

then

$$\dot{V} = r^T \left[E_C (\dot{x}_d + \Lambda e) + E_M (\ddot{x}_d + \Lambda \dot{e}) + E_G\right] - K_r |r|, \tag{22}$$

where $K_r = \mathrm{diag}[k_{rii}]$, $k_{rii} > 0$, $i = 1, \ldots, n$.

Let k_{rii} satisfy the following inequality:

$$k_{rii} > \left|E_C\right|_{\max} \left|\dot{x}_d + \Lambda e\right| + \left|E_M\right|_{\max} \left|\ddot{x}_d + \Lambda \dot{e}\right| + \left|E_G\right|_{\max} \left|x_d\right|, \tag{23}$$

then, we get

$$\ddot{V} < 0. \tag{24}$$

To verify the superiority of the SM-PI algorithm, still take the previous cases in Figure 3 as an example. Figure 4 illustrates the displacements (position signal tracking curves) and velocities (speed signal tracking curves) of flap(z)/lead-lag(y) motions, and the signals of control inputs, which are controlled by the nominal SMC algorithm based on upper bound method. Compared with those demonstrated in Figure 3, it can be seen that the superiority of the SM-PI algorithm in Figure 3 is remarkable. Its advantages are not only reflected in the tracking effects of displacements and velocities, but also in the fluctuations of control input signals. The displacement tracking of the SMC algorithm based on the upper bound method is not perfect, while the velocity tracking is more fluctuating, which not only increases the negative effect of inertia force in the control process but also increases the negative effect of damping force, which makes the control process more complicated.

In particular, in the engineering application of blade control, the control input can be expressed as an external excitation process such as pitch motion or trailing-edge flap motion, which requires the fluctuation of the control input signal to be as stable as possible, and is beneficial to the realization of physics process. Especially, the actuation technology of the physical hardware with a large amplitude and a high frequency should be avoided as much as possible

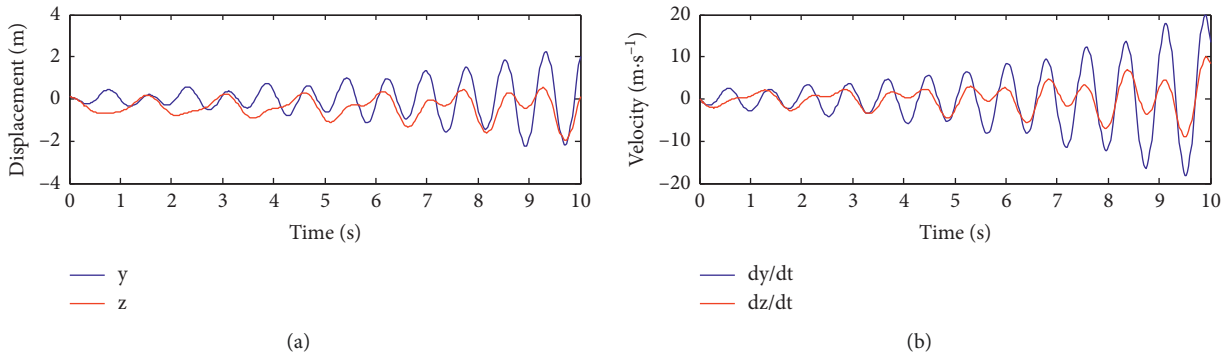

Figure 2: The uncontrolled divergent (a) displacements and (b) velocities of flap(z)/lead-lag(y) motions.

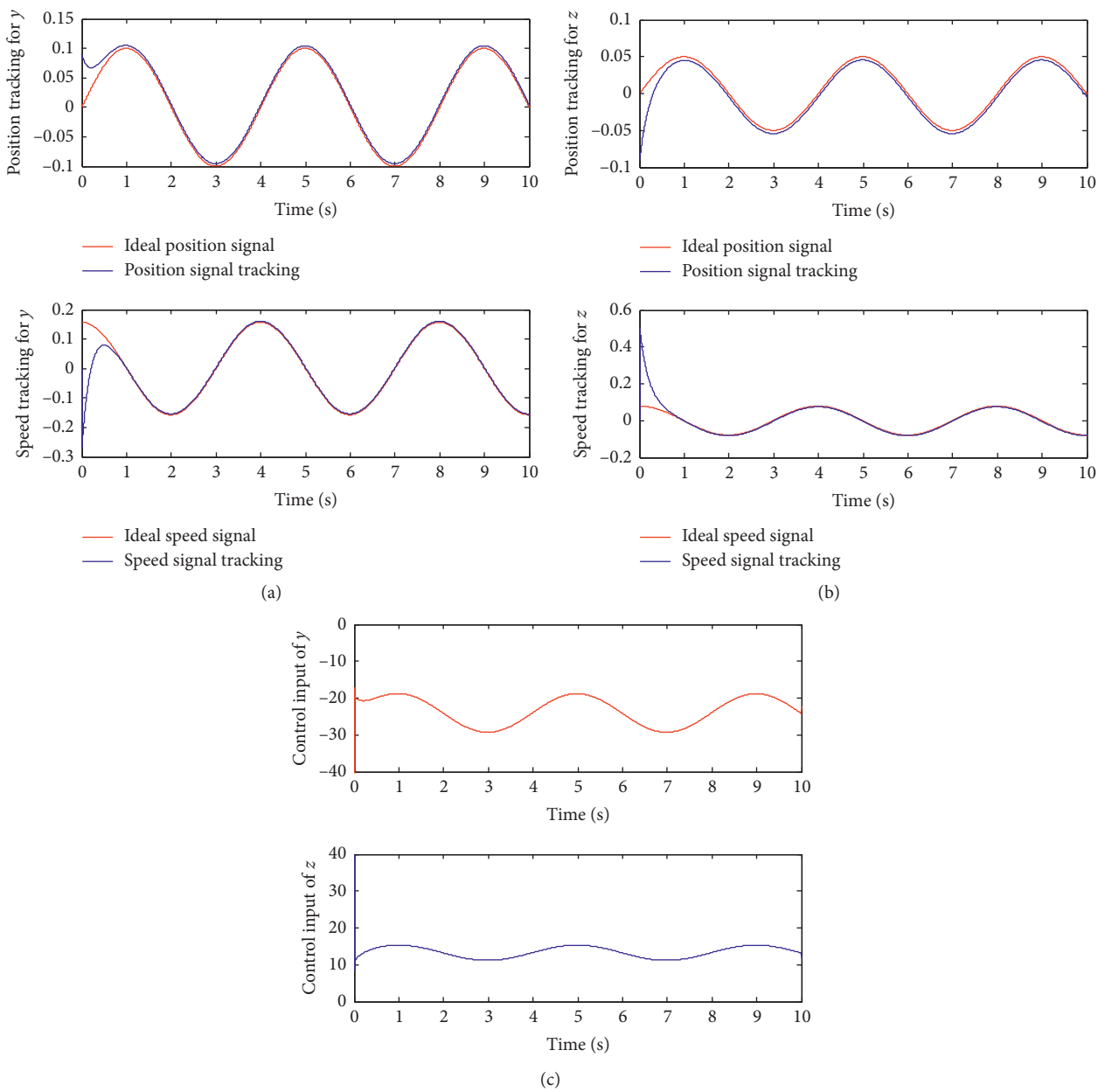

Figure 3: The controlled displacements (position signal tracking curves) and velocities (speed signal tracking curves) of flap(z)/lead-lag(y) motions, and the signals of control inputs, controlled by using the SM-PI.

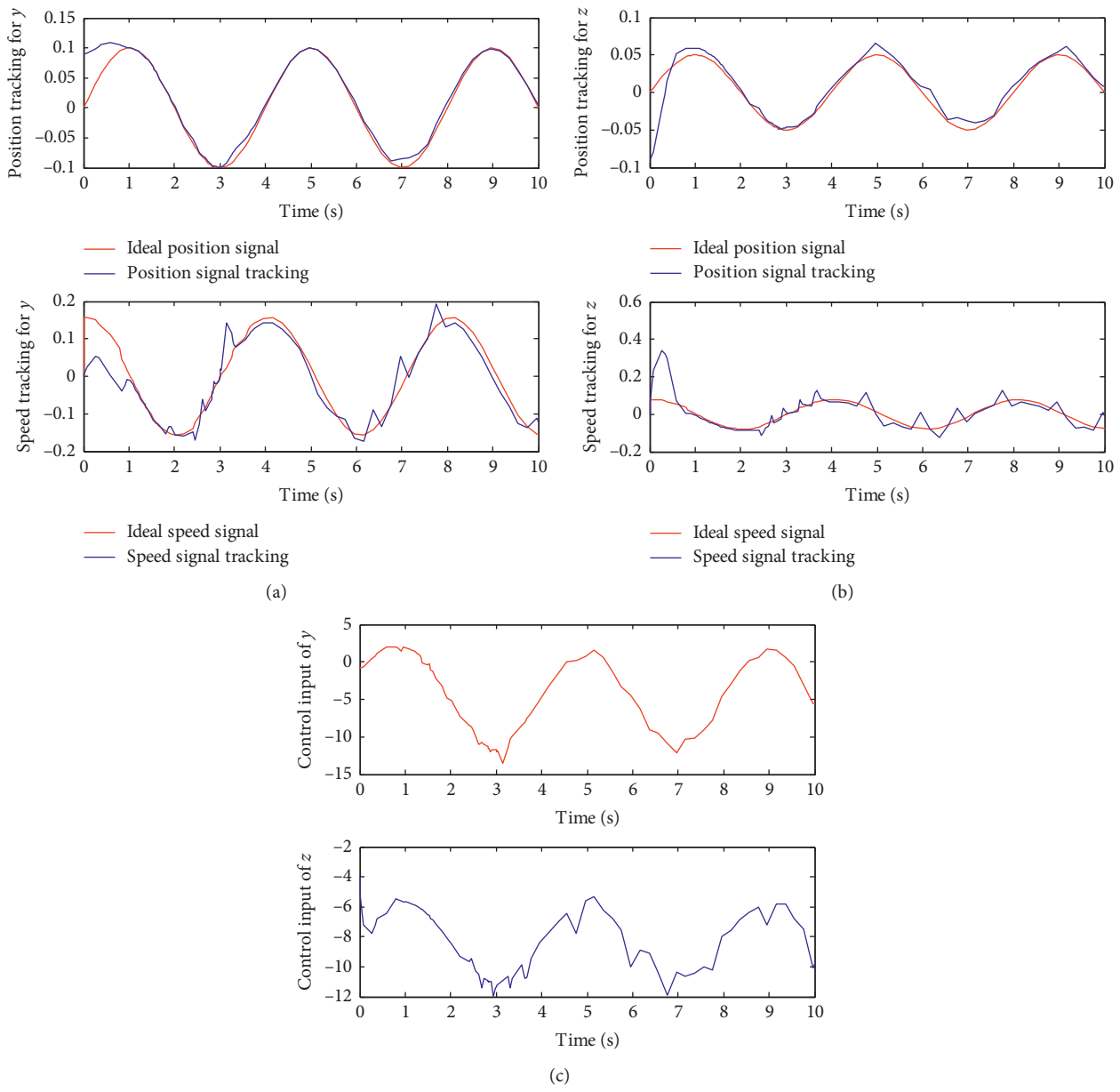

FIGURE 4: The displacements (position signal tracking curves) and velocities (speed signal tracking curves) of flap(z)/lead-lag(y) motions, and the signals of control inputs, controlled by the nominal SMC algorithm based on the upper bound method.

during the realization of physics process. The SM-PI algorithm does exactly satisfy this condition.

5.2. Robustness of SM-PI Algorithm. The robustness of the algorithm is also very important in the real-time control process. If a control interference signal τ_{id} is added into equation (4), it can be rewritten as

$$M_0\ddot{x} + C_0\dot{x} + G_0(x) = \tau - \tau_{\mathrm{id}}. \tag{25}$$

To increase the damping effect in the control process, we might as well relate τ_{id} and the change of velocity, and then τ_{id} can be expressed as $\tau_{\mathrm{id}} = \tau_d \mathrm{sign}(\dot{x})$. The item E in equation (11) can be expressed as

$$E = E_{\mathrm{M}}\ddot{x}_r + E_{\mathrm{C}}\dot{x}_r + E_{\mathrm{G}} + \tau_{\mathrm{id}}. \tag{26}$$

Figure 5 demonstrates the displacements of flap(z)/lead-lag(y) motions and the signals of control inputs, under conditions of $\tau_d = 0,\ 5,\ 10$, respectively. As far as the fluctuation of displacement and velocity is concerned, there is little difference in the results of these three cases ($\tau_d = 0,\ 5,\ 10$), which shows the robustness of the control effect. As far as the control input is concerned, there is a certain fluctuation of the input signals under the conditions of $\tau_d = 5$ and $\tau_d = 10$ compared with $\tau_d = 0$ (non-interference state). However, the fluctuation is not violent, and it is still within the physical realizable range, which shows the feasibility of the control process under the

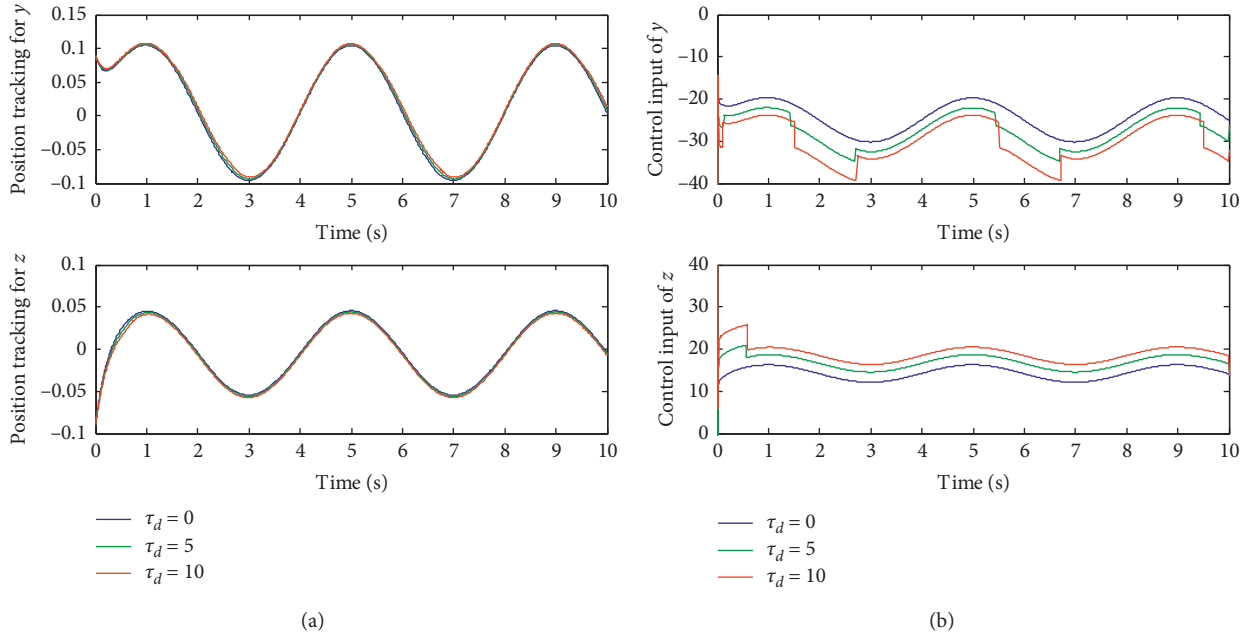

FIGURE 5: The displacements of flap(z)/lead-lag(y) motions and the signals of control inputs, under conditions of $\tau_d = 0, 5, 10$, respectively.

interference conditions. In short, the robustness of the SM-PI algorithm can be verified.

In particular, it is verified that the aerodynamic instability control, under the structural parameters conditions of the controlled object and the parameters cases of external wind speeds U that are fluctuating properly within a certain range, can achieve ideal control effects, which shows the robustness of the SM-PI algorithm. In addition, in this design, the wind speed U is $10\,\mathrm{m{\cdot}s^{-1}}$. This is due to the fact that the wind speed does not exceed $10\,\mathrm{m{\cdot}s^{-1}}$ when the turbulence intensity is constant and the surface roughness is specific, and the turbulence fractal characteristics are within 80 m height [18]. Of course, the SM-PI algorithm is fully applicable to the cases of $U < 10\,\mathrm{m{\cdot}s^{-1}}$, which is not discussed here.

5.3. Convergence Control of SM-PI Algorithm. In some engineering problems, the stability control of displacement is strict; for example, the displacement converges to a specific value, accompanied by the smallest possible vibration frequency. The same is true for the vibration control of wind turbine blades under certain conditions for flutter suppression; for example, we might as well require both displacements to converge to zeros, that is, the ideal position signals $x_d(1) = x_d(2) = 0$. In fact, the tracking problem is more universal, and it can be reduced to a convergent stability problem as long as the control input is within a reasonable and operational range.

Still take the previous cases in Figure 3 as an example. Figure 6 illustrates the position tracking signals for both y and z and corresponding control inputs. From the convergence point of view, both controlled displacements converge fast and can tend to be the steady-state values within 1 s, which reflects the convergence control performance of the algorithm. Although the controlled displacement cannot converge completely to zero, there is a minimal offset, but the direction of the offset is exactly the same as that of actual situation of flap(z)/lead-lag(y) motions. In the actual motion of wind turbine blades, the flap(z) motion is positive, while the lead-lag(y) motion is reverse, which is more consistent with the aeroelastic stability requirement of the blades. From the point of view of the control performance, the control input also converges and can tend to be stable process. Although the frequency of the control input is very high, it is an unfavorable factor, and the amplitude of the control quantity is relatively small, which is within the realizable range of the control operation. High frequency and low amplitude in excitation process are also feasible in physical implementation for blade. For example, we can use the high-frequency reverse cylinder to drive the trailing-edge flap structure to realize the input of the control quantity. Therefore, the convergent stability control in the limit cases can also be guaranteed, which further reflects the effectiveness of the SM-PI algorithm.

6. Experimental Platform Based on OPC Technology

In view of the difficulties of wind tunnel testing in verifying 2D airfoils, an experimental platform based on human-computer interaction is implemented with the PI controller executed in Siemens s7-200 PLC hardware using OPC technology [15] to verify the effectiveness of the SM-PI algorithm. Figure 7 demonstrates the experimental planning and platform (a) and experimental results displayed in touch screen (b).

The experimental platform is characterized by a number of features. (1) The sliding mode algorithm and PI control are completely implemented in PLC. However, due to the

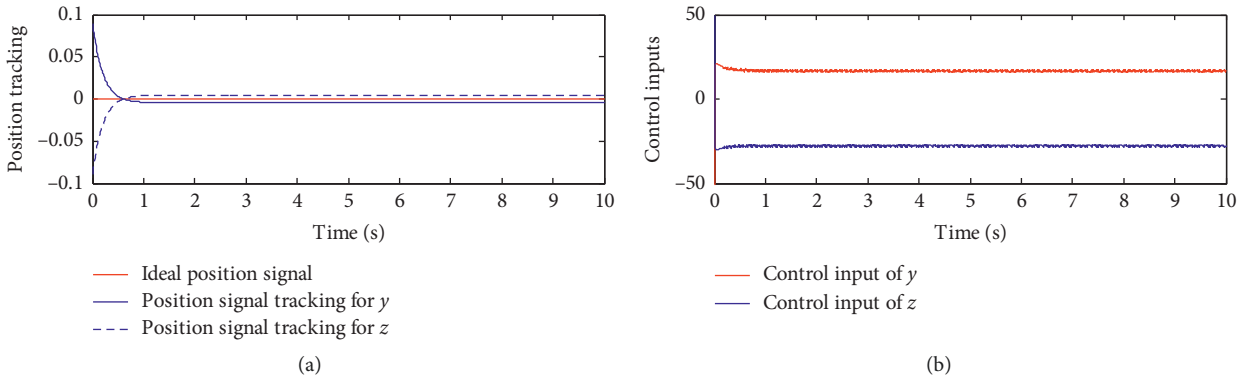

Figure 6: The position tracking signals for both y and z and corresponding control inputs under the condition of $x_d(1) = x_d(2) = 0$.

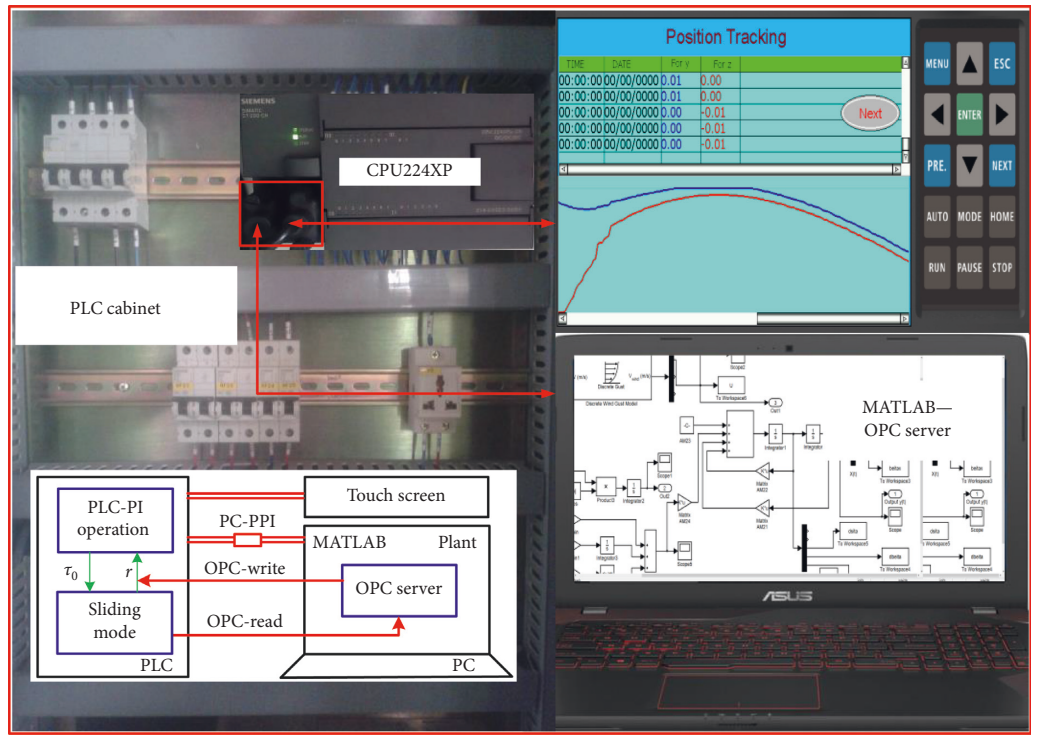

(a)

Figure 7: Continued.

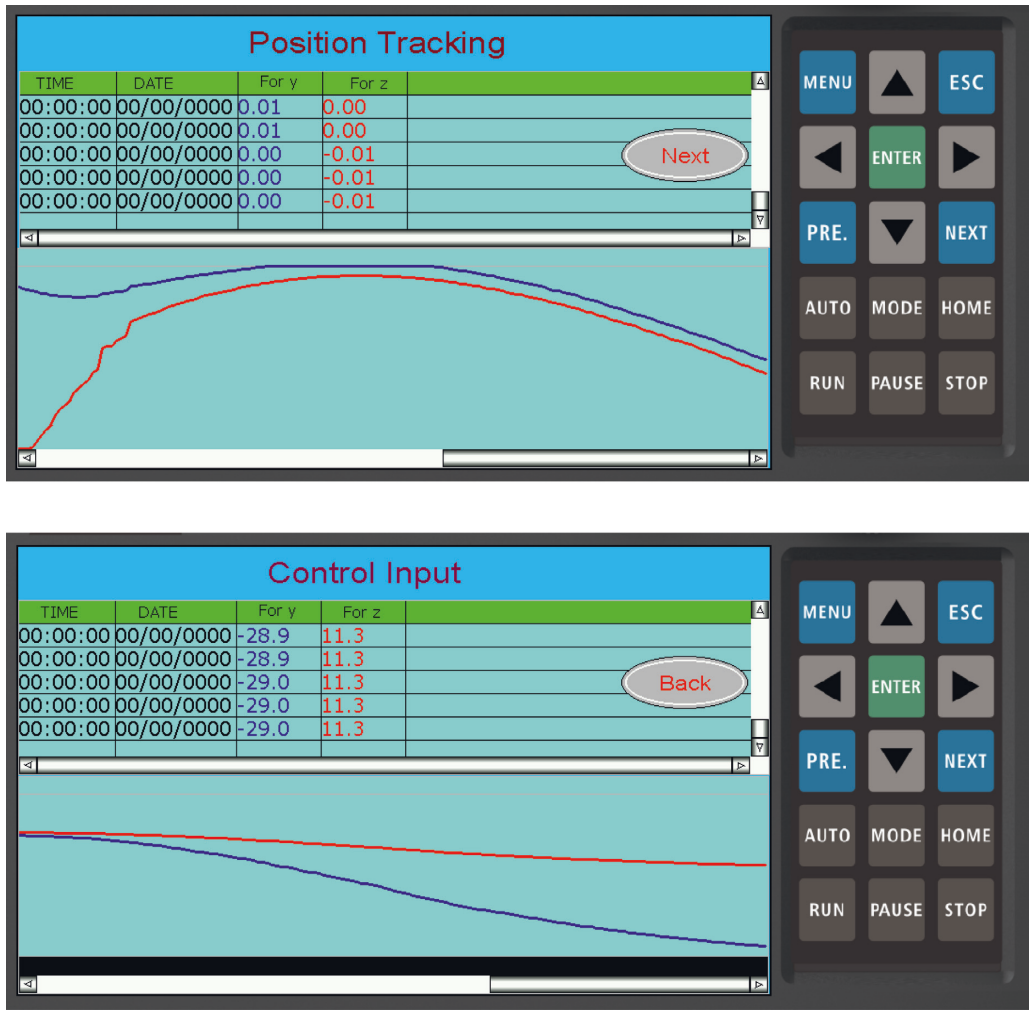

(b)

FIGURE 7: (a) The experimental planning and platform. (b) The experimental results displayed in human-computer interaction platform including position tracking signals for both y and z and corresponding control inputs.

limitation of CPU memory capacity, not all sliding mode algorithms (due to its complexity) can be run in PLC. After separating the nominal SMC algorithm from the PI control, the PLC has a built-in PI core program that can greatly simplify the SM-PI operation, which meets the real- time requirements of the control algorithm designed in the present study. In Figure 7(a), the internal signal transference of the SM-PI algorithm is also shown in the experimental planning; herein, $\tau_0 = \tau - \tau_m - \tau_\tau$, while the system model (plant) is fully run in PC. (2) The core of OPC technology is the OPC-Server, a built-in PC. It is based on the MATLAB simulation environment in PC and combines the OPC definition function of PC-Access software to realize it [15]. (3) The OPC technology realizes the data interactive transmission through the "read" and "write" operation of Server, and the "read" and "write" operation is realized through the PC-PPI cable. For technical operation and detailed configuration of OPC technology and communication parameters, please refer to [15]. (4) The touch screen (TS) connected to the 485 serial port in PLC is used to display the result signals.

In addition, it needs to be explained that the tuning of PI parameters (K_{p0} and K_{i0}) is carried out directly in the programming software of PLC. In the programming software of S7-200 PLC CPU, the manual setting and adjustment of PI parameters can be realized after opening the control panel of PID adjustment by using OPC technology. From the displacement fluctuation curve shown in the panel, the rationality of PI parameters can be determined. Once the parameters are determined, they can be fixed in the system and used as permanent PI parameters. Because of the use of OPC technology, this can actually be regarded as an "online" and real-time tuning process of parameters. The PI operation itself is a more complex integration process and feedback process. Due to the limitation of PLC memory and its scanning cycle, the program codes of PLC cannot be too long and complex. Otherwise, a relatively slow cycle time would take place as depicted in [15], which will result in an

increasing in the number of CPU modules, thus increasing cost and complexity of operating technique. Because PLC has a built-in PI operation module, it only needs to write the obtained PI parameter to the corresponding memory. The sliding mode operation and the PI controller only need to realize the data exchange between the two parties, which also greatly simplifies the programming of the software, and is an advantage of the SM-PI algorithm over the pure SMC algorithm.

Still take the previous cases in Figure 3 as an example. Figure 7(b) illustrates the position tracking signals for both y and z and corresponding control inputs. Since the signal presentation in TS is dynamic, one frame image of the position tracking only displays the flap(z)/lead-lag(y) fluctuations within time 0~2 s. Compared with the position tracking fluctuations in Figure 3, perfect consistency is reflected in the fluctuating trends. At the same time, it also shows the dynamic results of the fluctuation values, which scroll along with the action of the vertical scroll bar. Similarly, the control input image illustrates the extracontrol force τ for both displacements within time range of 1 s~3 s. Compared with those in Figure 3, it embodies perfect consistency.

The human-computer interaction platform vividly shows the implementation process of the SM-PI algorithm in the controller hardware, and it also provides a useful way to test the feasibility of the intelligent control algorithm in practical engineering application.

In addition, the OPC technology is actually a kind of virtual sensing and testing technology, the object of which is the system which has positive theoretical significance but cannot be built on the basis of practical entity. It virtualizes the roles of the sensor, the A/D module, the D/A module, and the transmission of the signal that is accomplished by the read-write programs of the OPC technology. The experimental results related to vibration-based health monitoring and control of the 2D blade system provide a simple and fast channel for qualitative analysis of vibration control of a 3D blade body.

7. Conclusions

In this study, vibration control for flap-wise and lead-lag displacements of the wind turbine blade section integrated with structural damping, based on the SM-PI tracking algorithm, is investigated by theoretical derivation and numerical simulation. Some concluding remarks including novelty and practicality can be outlined as follows:

(1) Structure model is a 2D damping-integrated section model. The aerodynamic coefficients are fitted to Fourier series expressions, which can eliminate the aerodynamic nonlinear problem directly, so as to facilitate the subsequent linear control process. Realization of vibration control is based on the SM-PI tracking algorithm, with controller design and stability analysis described.

(2) The SMC algorithm is based on the nominal model suitable for error tracking, which is integrated in the PI controller to facilitate implementation in a PLC controller hardware. Numerical simulation shows the effectiveness of position tracking and the feasibility of external control force. The superiority of the SM-PI algorithm is verified by comparison of another nominal SMC algorithm. The robustness is also verified by analysis of time responses under different control disturbances.

(3) The experiment based on human-computer interaction platform is carried out to testify the effects of the SM-PI method and the feasibility of the control algorithm in practical engineering application. Herein, the OPC technology plays an important role. OPC technology not only can be used to check the real-time effect of control theory but also can realize the "on-line" parameter tuning of K_{p0} and K_{i0} in the PI controller because of the high performance of program realization module of PID algorithm built in PLC CPU hardware.

Data Availability

The data used to support the findings of this study are available from the corresponding author upon request.

Conflicts of Interest

The author declares that there are no conflicts of interest regarding the publication of this article.

Acknowledgments

This work was supported by the National Natural Science Foundation of China (Grant no. 51675315).

References

[1] T. Liu, "Aeroservoelastic pitch control of stall-induced flap/lag flutter of wind turbine blade section," *Shock and Vibration*, vol. 2015, Article ID 692567, 20 pages, 2015.

[2] C. Gao, W. Zhang, and Z. Ye, "Numerical study on closed-loop control of transonic buffet suppression by trailing edge flap," *Computers & Fluids*, vol. 132, pp. 32–45, 2016.

[3] N. Li, M. J. Balas, P. Nikoueeyan, H. Yang, and J. W. Naughton, "Stall flutter control of a smart blade section undergoing asymmetric limit oscillations," *Shock and Vibration*, vol. 2016, Article ID 5096128, 14 pages, 2016.

[4] D. Song, J. Yang, M. Dong, and Y. H. Joo, "Model predictive control with finite control set for variable-speed wind turbines," *Energy*, vol. 126, pp. 564–572, 2017.

[5] A. Jain, G. Schildbach, L. Fagiano, and M. Morari, "On the design and tuning of linear model predictive control for wind turbines," *Renewable Energy*, vol. 80, pp. 664–673, 2015.

[6] J. Zhang, B. Li, P. Yu et al., "Model prediction control based on state space for doubly-fed induction generator," *Power System Technology*, vol. 41, no. 9, pp. 2905–2909, 2017.

[7] K. Lochan, B. K. Roy, and B. Subudhi, "SMC controlled chaotic trajectory tracking of two-link flexible manipulator with PID sliding surface," *IFAC-PapersOnLine*, vol. 49, no. 1, pp. 219–224, 2016.

[8] R. Saravanakumar and D. Jena, "Validation of an integral sliding mode control for optimal control of a three blade variable speed variable pitch wind turbine," *International Journal of Electrical Power & Energy Systems*, vol. 69, pp. 421–429, 2015.

[9] D. Paul and C. Xiao, "What researchers have learned from fractured wind turbine blades, DTU Wind Energy," 2018, https://www.windpowerengineering.com/mechanical/blades/what-researchers-have-learned-from-fractured-wind-turbine-blades.

[10] T. Liu, *Dynamic Stall Aeroelastic Stability Analysis and Flutter Suppression for Wind Turbine Blade*, Golden Light Academic Publishing, Beau-Bassin, Mauritius, 2017.

[11] S. Chakrabarty and A. Bartoszewicz, "Improved robustness and performance of discrete time sliding mode control systems," *ISA Transactions*, vol. 65, pp. 143–149, 2016.

[12] D. Haibo, Y. Xinghuo, M. Z. Q. Chen, and S. Li, "Chattering-free discrete-time sliding mode control," *Automatica*, vol. 68, pp. 87–91, 2016.

[13] S.-H. T. Jason, J.-S. Fang, J.-J. Yan et al., "A discrete DSMC was presented for the robust chaos suppression of the generalized continuous-time chaotic systems subject to matched/mismatched disturbances," *Nonlinear Analysis: Hybrid Systems*, vol. 29, pp. 74–84, 2018.

[14] B. Rahmani, "Robust output feedback sliding mode control for uncertain discrete time systems," *Nonlinear Analysis: Hybrid Systems*, vol. 24, pp. 83–99, 2017.

[15] T. Liu, "System modeling and instability control of wind turbine blade based on hydraulic pitch system and radial basic function neural network proportional-integral-derivative controller," *Proceedings of the Institution of Mechanical Engineers, Part I: Journal of Systems and Control Engineering*, vol. 232, no. 10, pp. 1412–1428, 2018.

[16] P. K. Chaviaropoulos, "Flap/lead-lag aeroelastic stability of wind turbine blade sections," *Wind Energy*, vol. 2, no. 2, pp. 99–112, 1999.

[17] J. Liu, *Sliding Mode Control Design and MATLAB Simulation*, Tsinghua University Publishing Company, Beijing, China, 2nd edition, 2012.

[18] Q. Yuan, C. Li, Y. Yang et al., "Research on comparison of the fractal characteristics of turbulent wind," *Acta Energiae Solaris Sinica*, vol. 39, no. 7, pp. 2027–2035, 2018.